High bandwidth flatness-based control of a PM-motor with protections in case of saturations

Alexandre Battiston[1,2], El-Hadj Miliani[1], Jean-Philippe Martin[2], Babak Nahid-Mobarakeh[2], Serge Pierfederici[2], Farid Meibody-Tabar[2]

1. IFP Énergies nouvelles
1,4 avenue de Bois Préau
92852 Rueil-Malmaison Cedex, France
alexandre.battiston@ifpen.fr

2. Université de Lorraine - Laboratoire GREEN
2, avenue de la Forêt de Haye
54500 Vandœuvre-Lès-Nancy, France

ABSTRACT. *This paper deals with a flatness-based control of a Permanent Magnet Synchronous Machine fed by a Voltage Source Inverter. This control method offers some benefits in both transients states and bandwidth terms. Although one-loop control architecture is proposed, some improvements to saturate the state variables are discussed to prevent the system from having any uncontrollable behavior and thus to ensure its robustness when disturbances occur.*

RÉSUMÉ. *Ce travail traite de la commande par platitude différentielle d'un système de traction électrique muni d'un onduleur de tension et d'une machine synchrone à aimants permanents. La maîtrise des régimes transitoires ainsi que la rapidité de commande (à une boucle) sont autant d'arguments pour l'application de ce contrôle sur le système présenté. Puisque les courants côté machine ne sont pas directement contrôlés, cet article propose des solutions permettant de vaincre les phénomènes d'emballement et d'assurer la saturation des grandeurs d'état le cas échéant.*

KEYWORDS: *differential flatness, PMSM, voltage source inverter, large signal control, saturation, transients.*

MOTS-CLÉS : *platitude différentielle, MSAP, onduleur de tension, commande large signal, saturation, transitoires.*

DOI:10.3166/EJEE.17.115-132 © Lavoisier 2014

1. Introduction

Flatness-based control (Fliess *et al*., 1995; Lévine, 2009; Hagenmeyer, Delaleau, 2003) offers numerous benefits compared to the conventional controls. Among these latter, the cascaded linear PI regulators (Kaiqi, 2011; Su *et al*., 2005) or other robust regulators based on sliding-mode control (Zhang *et al*., 2013; Feng *et al*., 2009) can be cited. Some advantages can be enumerated:

– Theoretically, if all parameters are well-known, differential flatness can work in open-loop without any feedback linearization. But in experimental cases, parameters cannot be perfectly known and additional regulators based on feedback laws are added to the control chain. These feedback laws allow stabilizing the real trajectories around their predicted trajectories. Both the parameters uncertainties and the modeled errors thus can be rejected. It is important to point out that flatness is different from dynamic feedback linearization (Martin *et al*., 2002). Flatness is a property of non-linear systems and its purpose is not to transform the system via a variable change. It does not transform nonlinear systems into linear ones but all the nonlinearities are conserved.

– If the system shares flatness properties, all the state or command variables can be expressed as a function of a chosen *flat output* and its successive derivatives without any differential integration.

– It is possible to reduce the noise on variables by considering the calculated references instead of the measured values.

– The chattering effect that may occur when a sliding-mode control is used does not exist anymore when an operating point is changed (Payman *et al*., 2011).

– The trajectory planning step offers better performances over the conventional control on both regulation and trajectory tracking terms (Payman, 2009; Gensior *et al*., 2009).

– In (Dannehl, Fuchs, 2006), a cascaded (two loops) flatness-based control is applied to an induction motor and results show that the performances are always competitive with the conventional control.

– As regards robustness and parameters uncertainties, the performances have been proved in (Houari *et al*., 2012).

It is proposed in this paper to implement a centralized control based of flatness properties of a permanent magnet synchronous machine (PMSM). This has been first proposed in (Delaleau, Stanković, 2004) using a two-loop control also known as hierarchical control. The latter PMSM is fed by a DC-source voltage v_s with its passive filter $L_f C_f$. The system is presented in Figure 1 and parameters are given in Table 1. Hereinafter, the passive filter will be modeled by a simple DC-source voltage assuming that the passive elements are well-sized to suppose the voltage across the DC-link capacitor C_f is not impacted by the load.

One-loop flatness-based control is implemented to improve the bandwidth of the control. Thus, some variables are not directly controlled and problems in case of command saturations are taken into account to protect the system and prevent him

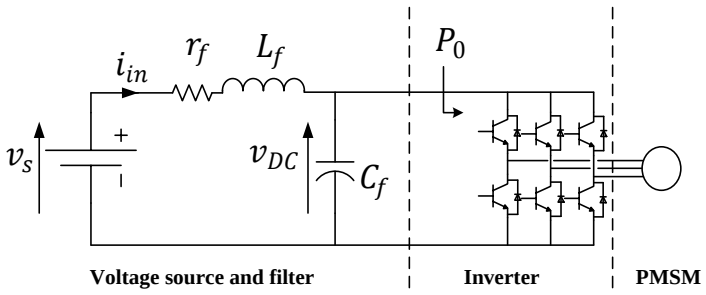

Figure 1. Electric traction system using a PMSM and a voltage source inverter fed by a DC-source voltage

from becoming uncontrollable. These additional corrections are based on anti-windup schemes (Shin, Park, 2012; Ghoshal, John, 2010; Malloci, 2006; Richter, De Doncker, 2011).

Flatness properties of the considered system as well as the trajectory planning step are presented and detailed in section 2. In section 3, experimental results validate simulation ones. Finally in section 4, the saturation issues are taken into account and corrected with the help of different saturation methods.

Table 1. Symbols description

Symbol	Description
v_s	DC-source voltage
v_{DC}	DC-bus voltage
P_0	Absorbed power by the inverter
r_s	Stator resistor
$l_d = l_q$	Stator inductors
ψ_f	Permanent magnet flux
Ω	Mechanical speed
J	Inertia coefficient
T_s	Load torque
f	Friction coefficient
p	Number of poles pairs

2. Control strategy description

2.1. Flatness property

Basically, a state model with a state vector x and an input vector u defined by $\dot{x} = f(x, u)$ with $x \in \mathbb{R}^n$ and $u \in \mathbb{R}^m$, is a *flat system* if it exists a *flat output* $y \in \mathbb{R}^m$

such that $y = h_y\left(x, u, \dot{u}, \ddot{u}, ..., u^{(q)}\right)$ where x and u can be written in terms of the flat output y and its derivatives $\dot{y}$, $\ddot{y}$, ... :

$$x = h_x\left(y, \dot{y}, \ddot{y}, ..., y^{(r)}\right)$$

$$u = h_u\left(y, \dot{y}, ..., y^{(r+1)}\right)$$

Functions $h_y : \mathbb{R}^n \times (\mathbb{R}^m)^{q+1} \longmapsto \mathbb{R}^m$, $h_x : (\mathbb{R}^m)^{r+1} \longmapsto \mathbb{R}^n$, and $h_u : (\mathbb{R}^m)^{r+2} \longmapsto \mathbb{R}^m$ are supposed to be regular. More details can be found in (Hagenmeyer, Delaleau, 2003; Lévine, 2009). The system presented in Figure 1 can be modeled by the state system (1).

$$\frac{d}{dt}\begin{bmatrix} i_d \\ i_q \\ \Omega \end{bmatrix} = \begin{bmatrix} \frac{1}{l_d} \cdot (-r_s\, i_d + v_d + p\,\Omega\, l_q\, i_q) \\ \frac{1}{l_q} \cdot (-r_s\, i_q + v_q - p\,\Omega\, (l_d\, i_d + \psi_f)) \\ \frac{1}{J} \cdot (p\,\psi_f\, i_q - T_s - f\,\Omega) \end{bmatrix} \tag{1}$$

Thus, the state and input vectors are defined according to (2) and (3) respectively.

$$x = [i_d, i_q, \Omega]^T \in \mathbb{R}^3 \tag{2}$$

$$u = [v_d, v_q]^T \in \mathbb{R}^2 \tag{3}$$

Since the input vector (3) has two components, the flat output order has to be the same. It is proposed to consider the mechanical speed Ω and the d-axis flux $\psi_d = l_d\, i_d + \psi_f$ (4) as flat output components:

$$y = \begin{cases} y_\Omega = \Omega \\ y_d = \psi_d \end{cases} \tag{4}$$

Flatness properties of the system can now be verified by expressing all the state and input variables in terms of these flat output components. One obtains (5) and (6) that proves the system shares flatness properties.

$$\begin{cases} i_d = \dfrac{\psi_d - \psi_f}{l_d} = h_{i_d}(y_d) \\ i_q = \dfrac{1}{p\,\psi_f}\,(J\,\dot{y_\Omega} + T_s + f\,y_\Omega) = h_{i_q}(y_\Omega, \dot{y_\Omega}) \\ \Omega = y_\Omega = h_\Omega(y_\Omega) \end{cases} \tag{5}$$

$$\begin{cases} v_d = \dot{y_d} + r_s\, h_{i_d}(y_d) - p\, y_\Omega\, l_q\, h_{i_q}(y_\Omega, \dot{y_\Omega}) = h_{v_d}(y_d, \dot{y_d}, y_\Omega, \dot{y_\Omega}) \\ v_q = l_q\, \dfrac{d}{dt} h_{i_q}(y_\Omega, \dot{y_\Omega}) + r_s\, h_{i_q}(y_\Omega, \dot{y_\Omega}) + p\, y_\Omega\, (l_d\, h_{i_d}(y_d) + \psi_f) \\ \qquad\qquad = h_{v_q}(y_\Omega, \dot{y_\Omega}, \ddot{y_\Omega}, y_d) \end{cases} \tag{6}$$

2.2. Trajectory planning

Trajectory planning represents an important step for the implementation of flatness-based control. Previously, flatness properties allowed all the state and input variables to be written as a function of a chosen flat output y (5) and (6). That is the flat output trajectory defines all the state or input variables trajectories. It is thus interesting to propose a well-known mathematical form so that all the transient state behaviors can be predicted. Two criteria have been considered to make that choice:

– The trajectory has to be simple enough to easily calculate some remarkable values. For instance, the peak value of the q-axis current at the machine start.

– The trajectory has to be continuously adapted to any speed reference changes.

According to the latter criteria, a second order filter is chosen for the speed reference trajectory. With a damping coefficient $\xi = 1$, the solution is given by (7):

$$y_\Omega^*(t) = y_\Omega^\infty \left(1 - (1 + \omega_0\, t)\, e^{-\omega_0\, t}\right) \tag{7}$$

where y_Ω^∞ represents the step value, and ω_0 the pseudo-pulsation. This latter is designed according to response time and overshoot data. Note that the d-axis flux trajectory can be identical.

2.3. One-loop flatness-based control and regulation parameters

In most cases, the machine parameters are not exactly known and regulators have to be inserted within the control scheme to reject some parameters uncertainties. In this paper, one-loop control is proposed in which the control system returns an input vector $u = [v_d, v_q]^T$ for a given reference vector $y^* = [y_\Omega^*, y_d^*]^T$. In order to be less dependent on the measurement noise, the components of the input command u (6) are calculated with the reference values y_Ω^* and y_d^* instead of their measured values y_Ω and y_d. To implement regulators, two new variables are defined. They correspond to the higher order derivative terms of the flat output components expressed in u. That is:

$$\begin{cases} \mu_\Omega = \ddot{y_\Omega} \\ \mu_d = \dot{y_d} \end{cases} \tag{8}$$

Two additional control laws are thus defined to make the errors $\epsilon_\Omega = y_\Omega^* - y_\Omega$ and $\epsilon_d = y_d^* - y_d$ converge to zero according to the following trajectories:

$$\begin{cases} \ddot{y_\Omega}^* - \mu_\Omega + k_{\Omega_1} \cdot (\dot{y_\Omega}^* - \dot{y_\Omega}) + k_{\Omega_2} \cdot (y_\Omega^* - y_\Omega) + k_{\Omega_3} \cdot \int (y_\Omega^* - y_\Omega) d\tau = 0 \\ \dot{y_d}^* - \mu_d + k_{d_1} \cdot (y_d^* - y_d) + k_{d_2} \cdot \int (y_d^* - y_d) d\tau = 0 \end{cases} \tag{9}$$

The integral terms in (9) are present to reject both the modeling errors and the parameters uncertainties. An identification with second order systems parameters leads

to the expression of the regulation parameters (10). These latter are designed so that performance criteria meet the requirements (response time, overshoot, etc...).

$$\begin{cases} k_{\Omega_1} = 2\,\xi\,\omega_\Omega - p_\Omega \\ k_{\Omega_2} = \omega_\Omega^2 - 2\,\xi_\Omega\,p_\Omega\,\omega_\Omega \\ k_{\Omega_3} = -p_\Omega\,\omega_\Omega^2 \\ k_{d_1} = 2\,\xi_d\,\omega_d \\ k_{d_2} = \omega_d^2 \end{cases} \tag{10}$$

Note that the real pole p_Ω is chosen so that its influence does not impact the second order behavior. ξ_Ω and ξ_d as well as ω_Ω and ω_d represent the damping coefficients and the pulsations (control bandwidths) respectively. The proposed control scheme is presented in Figure 2. The *passive saturation block* will be presented below.

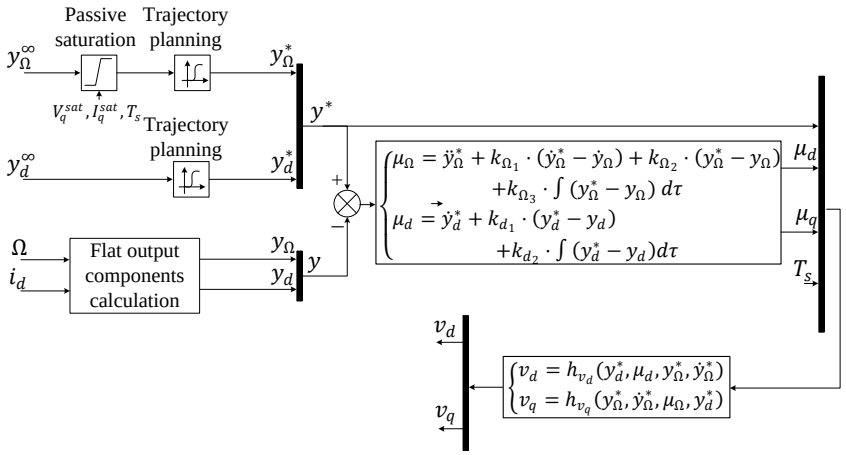

Figure 2. Proposed one-loop flatness-based control scheme

3. Validation of the control strategy

3.1. Experimental and simulation results

An experimental test bench, presented in Figure 3, is realized to validate the proposed flatness-based control. It is composed of a PMSM fed by a voltage source inverter. Global control is implemented on a dSPACE DS1005 processor programmable from Simulink. Both the switching and sampling frequencies have been fixed to 10 kHz. The PM-motor is mechanically coupled with another same PM-machine that is connected to a 3-phase resistor. This is equivalent to an experimental load torque that can be modeled by $\Gamma_{load} = f_r\,\Omega$ where f_r is an equivalent friction coefficient. The parameters used in both simulation and experiment are given in Table 2.

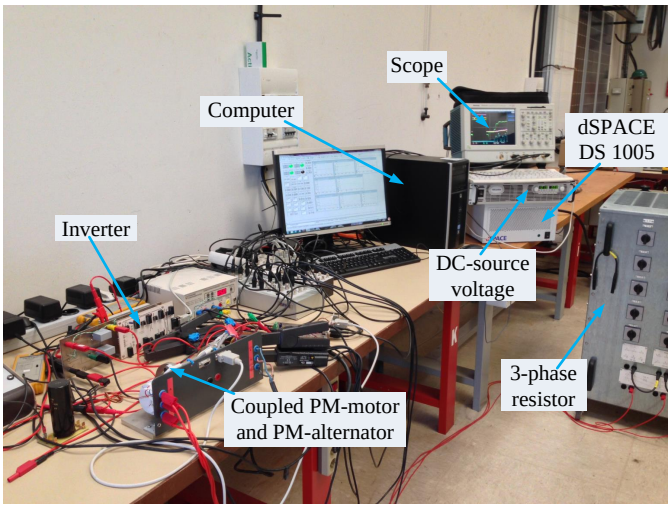

Figure 3. Experimental test bench

Table 2. Parameters quantities

Symbol	Quantity
$v_s \approx v_{DC}$	100 V
$l_d = l_q$	5 mH
ψ_f	0.075 Wb
p	4
r_s	1.8 Ω
J	$500 \cdot 10^{-7}$ kg m^2
f	$5 \cdot 10^{-4}$ Nms
f_r	0.0055 Nm
$\xi_\Omega = \xi_d$	0.8
ω_Ω	500 rad/s
ω_d	1000 rad/s
switching or sampling frequency	10 kHz

The waveforms obtained by simulation are plotted in Figure 4. They present the state variables response to a given speed profile. An important result is given by considering the q-axis current waveforms. Indeed, i_q follows perfectly its calculated trajectory $i_q^* = h_{i_q}(y_\Omega^*, \dot{y_\Omega}^*)$ without any current controller in the control scheme. It is verified that the calculated reference i_q^* is dependent on the speed reference trajectory y_Ω^*. This latter evolves according to a second order trajectory response as expected. As regards the d-axis current i_d, it is well-controlled to $i_d^* = 0$ via the control of the d-axis flux ψ_d.

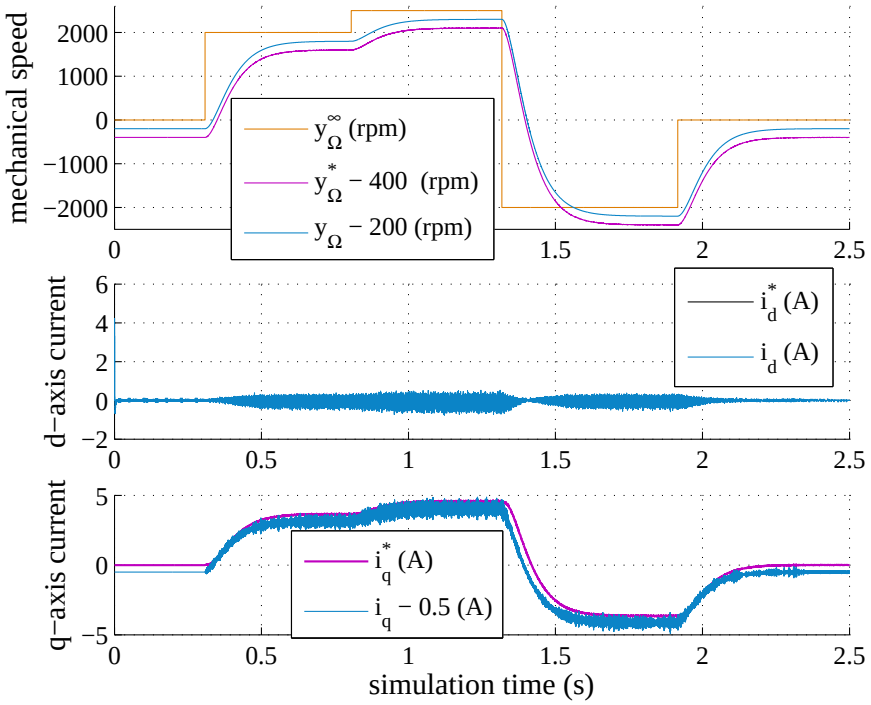

Figure 4. Simulation results in response to a speed profile

In Figure 5 and Figure 6 are presented some experimental results where variables are plotted in response to the same speed profile as in simulation case. These results allow validating the proposed control. As previously, the q-axis current follows its trajectory given by the speed controller and the d-axis current is well-controlled to zero.

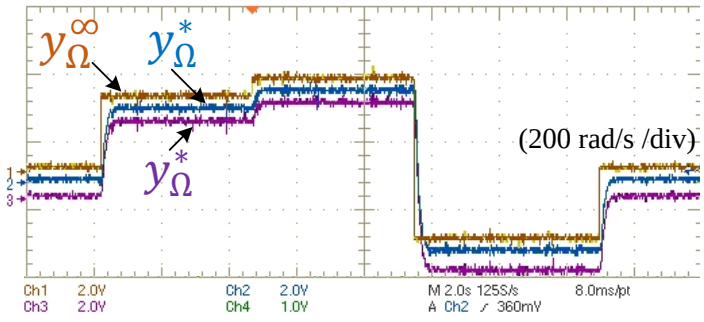

Figure 5. Experimental mechanical speed in response to a speed profile

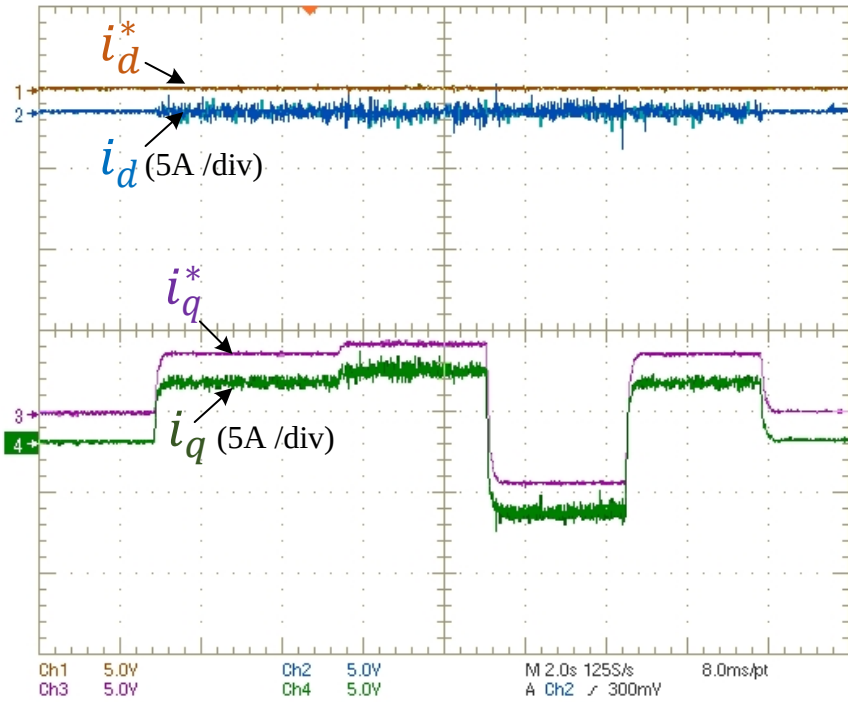

Figure 6. Experimental results of the dq-axis currents in response to a speed profile

4. Variables saturation: study and correction

One-loop control offers advantages in terms of speed control and bandwidth for regulation. The previous results show that the q-axis current perfectly follows its reference trajectory i_q^* without any current control loop in the controller scheme. These results are valid if variables are not saturating during the system process. For instance, an external load torque may cause the saturation of one or several variables (state or control variables) and the controllability of the machine may be lost. This section aims at proposing some corrections based on anti-windup schemes (Choi, Lee, 2009) in order to prevent the system from becoming uncontrollable. After a brief description of the windup phenomena, three saturation methods are proposed. The *passive saturation* aims at saturating some state or control variables by means of adapting the reference trajectory of the mechanical speed. The *active saturation* method helps to protect the system against external disturbances that may be faster than the speed trajectory response. These two first methods aims at focusing on keeping the controllability of the machine. By contrast, the third *max saturation* method acts when the system is facing an intensive disturbance. Its goal is to stop the system as a "emergency stop".

4.1. The windup phenomena

If one of the control variables (v_d or v_q) is saturating, it does not correspond anymore to the real one that should have been generated to control the system. Thus, a static error appears between the real value and its saturation. The integrators in (9) are going to accumulate it and the longer integration time, the more difficult the desaturation. That is why some methods, also known as anti-windup methods, have been developed to prevent the system from staying in an uncontrolled state of saturation. Two philosophies are generally taken into account. The first one allows the control command to saturate. The error is corrected *a posteriori* by acting on the integrators input. The second one works by anticipating all changes in the reference trajectory (for instance the one of the speed y_Ω^*). This latter philosophy will be taken into account in the following parts.

4.2. Passive saturation *method by adapting the reference trajectory*

This second philosophy is interesting as it does not introduce additional poles in the state model of the system. Thus, the system dynamic is not impacted by this method. It will be called *passive saturation* in the sections that follow.

4.2.1. Theoretical study

Two variables are considered. The q-axis current i_q as state variable and the q-axis voltage v_q as control command variable. These variables can be expressed in steady state by considering (5) and (6) and on the assumption that $i_d = i_d^* = 0$:

$$\begin{cases} V_q = h_{v_q}(y_\Omega^*) = r_s \dfrac{T_s + f\, y_\Omega^*}{p\,\psi_f} + p\, y_\Omega^*\, \psi_f & (11) \\ I_q = h_{i_q}(y_\Omega^*) = \dfrac{1}{p\,\psi_f}(T_s + f\, y_\Omega^*) & (12) \end{cases}$$

These quantities depend on both the reference trajectory of the mechanical speed y_Ω^* and the load torque parameter T_s, which is estimated. Experimentally, this latter is considered as a viscous torque whose modeling is given by $T_s = f_r\, \Omega$. If the torque has a constant component T_r, the model can be given by $T_s = F_r(\Omega)\, \Omega$ with $F_r(\Omega) = f_r + T_r/\Omega$. It is possible to write the inverse functions of (11) and (12) in order to express the mechanical speed saturation value. One obtains as a function of the known saturation values V_q^{sat} and I_q^{sat}:

$$\begin{cases} y_\Omega^{sat1}(V_q^{sat}) = \dfrac{V_q^{sat}}{(f + F_r(\Omega))\, \dfrac{r_s}{p\,\psi_f} + p\,\psi_f} & (13) \\ y_\Omega^{sat2}(I_q^{sat}) = \dfrac{p\,\psi_f\, I_q^{sat} - T_r}{f + f_r} & (14) \end{cases}$$

Finally, the reference step value y_Ω^∞ of the mechanical speed is modified by taking the minimum between (13) and (14):

$$(y_\Omega^\infty)_{sat} = \min\left(y_\Omega^{sat1}(V_q^{sat}), y_\Omega^{sat2}(I_q^{sat})\right) \tag{15}$$

4.2.2. Experimental results and validation

In order to validate the proposed *passive saturation*, some experimental tests are conducted and results are given in Figure 7. They are applied to the q-axis voltage v_q. For this test, the saturation value of v_q has been fixed to $V_q^{sat} = 30\,\text{V}$. The first speed step, identified by (1) in the figure, sets a voltage $v_q = 25\,\text{V}$. As this value is lower than V_q^{sat}, there is no need to saturate it and both the speed reference value y_Ω^* and its measured value y_Ω reach the set value y_Ω^∞. By contrast, the second speed step, identified by (2) in the figure, forces the q-axis voltage value to be superior to V_q^{sat}. Thus, the speed reference trajectory is modified so that the q-axis voltage is passively saturated according to (13). In Figure 7, v_q is well saturated to its saturation value and the controllability of the machine is preserved.

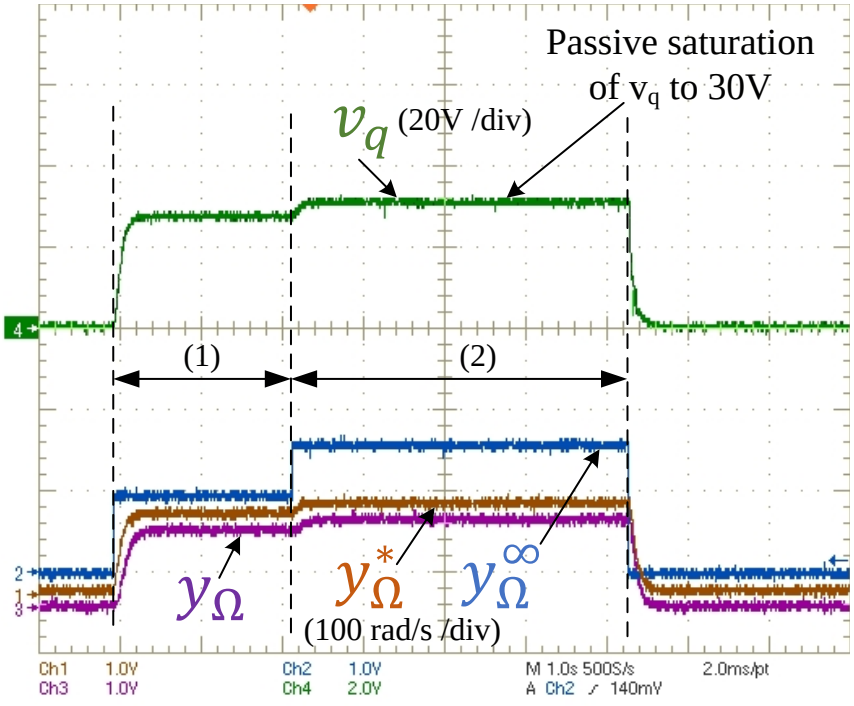

Figure 7. Passive saturation *of v_q to 30V*

4.3. Active saturation *method in case of disturbances*

The previous method is efficient while the machine is controllable. Now, if the machine runs at its limit of controllability, and if a disturbance occurs, other corrections has to be added. The *controllability* in this paper is defined by the fact that the DC-bus voltage v_{DC} is sufficient to control the machine. The controllability law can easily be expressed as follows for a Space Vector Modulation PWM strategy:

$$V_{\max} \leq \frac{v_{DC}}{\sqrt{3}} \quad \text{with} \quad V_{\max} = \sqrt{\frac{2}{3}}\sqrt{v_d^2 + v_q^2}$$

The expressions (13) and (14) depend on the saturation values V_q^{sat} and I_q^{sat} but also on the load torque estimation T_s. Generally, if a disturbance (load torque) is applied to the machine, its dynamic can be superior to that of the speed regulation. Thus, the *passive saturation* method might not be able to saturate fast enough the variables and some peak values might appear. It is thus proposed in the following section an *active saturation* method for completion of the passive one.

4.3.1. Active saturation of the q-axis current i_q

It is proposed to focus on the state variable i_q, which represents an image of the 3-phase currents in the machine windings and in the inverter switches. As the q-axis current is controlled by means of the q-axis voltage according to (16), the idea consists in immediately modifying the v_q voltage as soon as an overshoot is detected (that is $i_q \geq I_q^{sat}$).

$$l_q \frac{di_q}{dt} = -r_s\, i_q + v_q - p\,\Omega\,(l_d\, i_d + \psi_f) \tag{16}$$

If $i_q \geq I_q^{sat}$, the q-axis voltage v_q is modified as follows:

$$V_q^{mod} = r_s\, I_q^{sat} + p\, y_\Omega\, \psi_f \tag{17}$$

This latter equation (17) corresponds to the steady state value of the q-axis voltage that would lead to $i_q = I_q^{sat}$ (with $i_d = i_d^* = 0$). For additional protection, a v_q superior limit is defined (18) and it depends on the speed reference value y_Ω^* and on the estimation of the load torque T_s. A margin coefficient γ is added to overestimate the value (10% more).

$$V_q^{lim} = \left(r_s\, \frac{f\, y_\Omega^* + T_s}{p\,\psi_f} + p\, y_\Omega^*\, \psi_f\right) \cdot \gamma \tag{18}$$

4.3.2. Simulation results with active saturation *method*

A simulation is undertaken with both the passive and active saturation methods activated. Results are plotted in Figure 8. The saturation value of i_q has been fixed to $I_q^{sat} = 1.8\,\text{A}$ for the *passive saturation* method and 20 % more ($I_q^{sat2} = 2.16\,\text{A}$) for

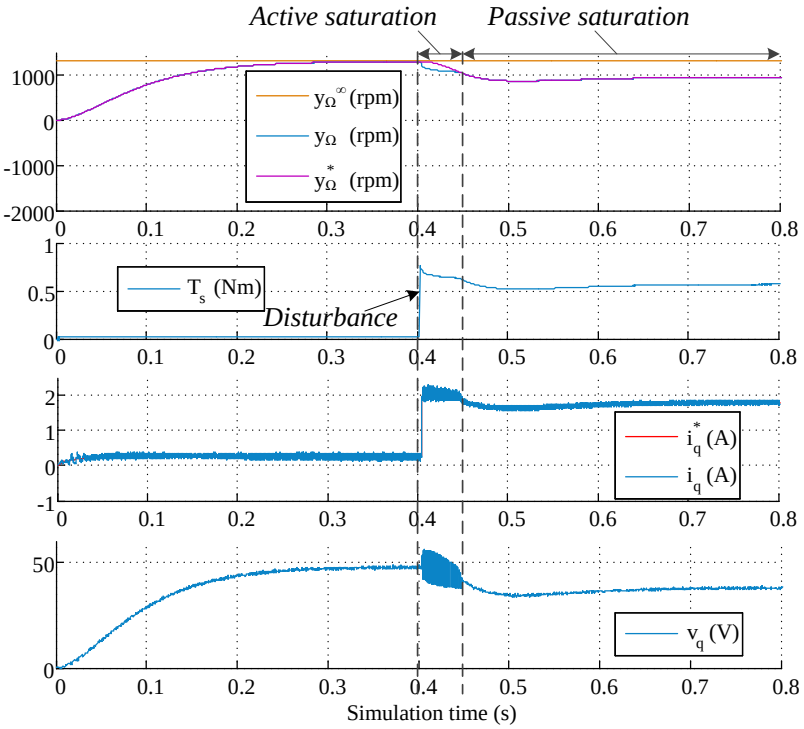

Figure 8. Disturbed system with both the passive and active saturation methods activated

the *active* one. When the disturbance suddenly occurs, the speed falls to a parasitic equilibrium point. This causes an increase in the q-axis voltage v_q, and so an increase in the q-axis current i_q. When the detection at 2.16 A is made, the *active saturation* method is automatically activated. This method is thus going to maintain the q-axis current in the vicinity of its saturation value (2.16 A) by switching v_q between the defined values (17) and (18). At this time, the integrators are immediately stopped and a change of speed reference is allowed so that the speed trajectory goes to the parasitic equilibrium point. After the trajectory gets back to the speed measured value, the controllability of the machine is restored and the *passive saturation* can act by saturating i_q to $I_q^{sat} = 1.8$ A. It is obvious the speed does not follow its set value y_Ω^∞ anymore. The main important is to preserve the controllability of the machine.

4.3.3. Experimental results with active saturation *method*

Figure 9 presents a similar test realized on the experimental test bench. When the load torque is suddenly applied to the machine, the q-axis current increases until the saturation value $I_q^{sat2} = 2.16$ A. The *active saturation* method is thus activated to maintain i_q in the vicinity of I_q^{sat2} by means of switching v_q between the two defined

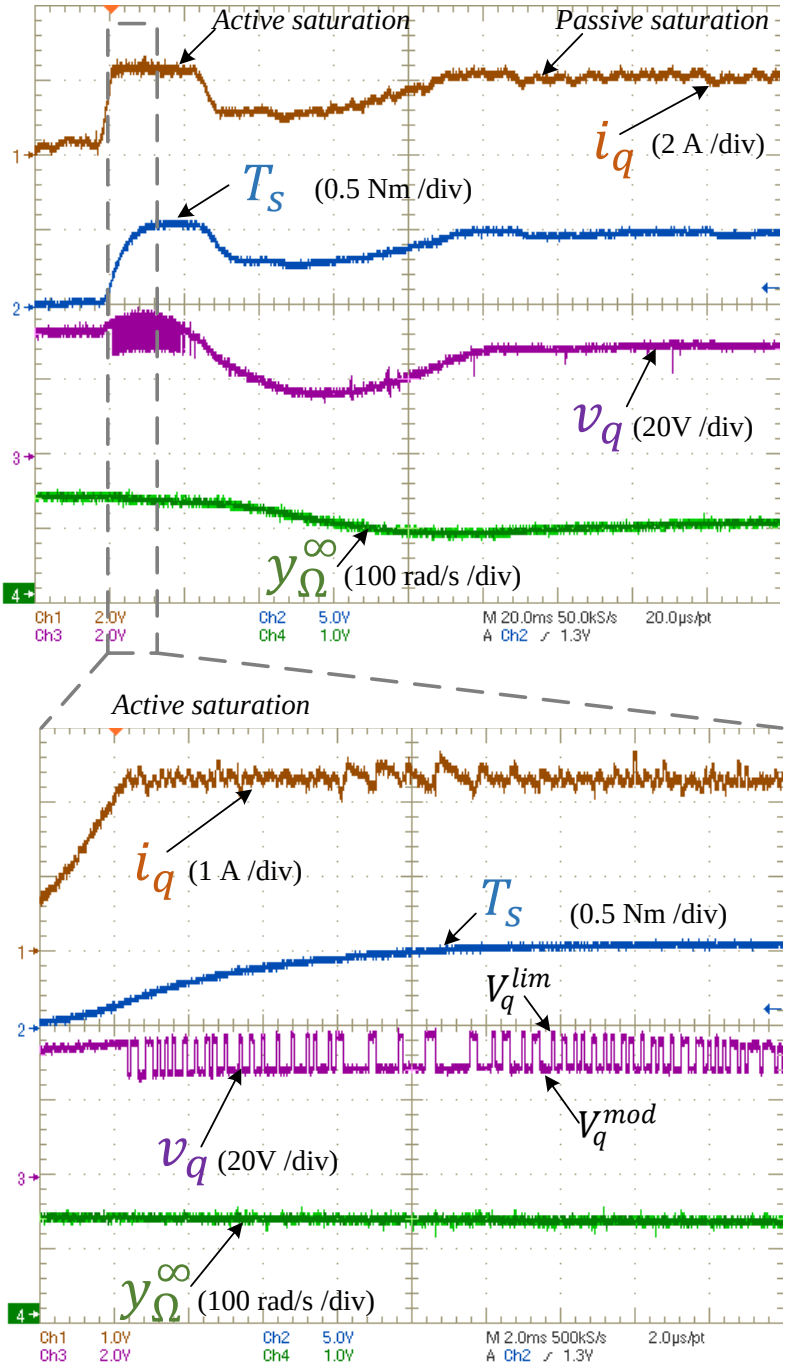

Figure 9. Experimental validation when both the active *and* passive saturations *work simultaneously*

values V_q^{mod} and V_q^{lim}. A zoom is given in the bottom of the figure which details the *active saturation* of i_q. This figure shows i_q is well-saturated. When the disturbance is applied, the speed reference is immediately changed so that the *active saturation* only last for a short period of time. The *passive saturation* is then automatically activated when the speed reference reaches the equilibrium point. The q-axis current is finally passively saturated to $I_q^{sat} = 1.8\,\text{A}$ and the control of the machine is maintained.

It is important to point out the two methods run simultaneously. In fact, the detection of different levels of i_q, defined by I_q^{sat} and I_q^{sat2}, determines which method has to be activated.

4.4. Max saturation *method*

If an intensive load torque is applied to the machine, a last resort method can be added. This third method, called *max saturation* method, aims at stopping the system and does not try to maintain its controllability. It takes into account the peak value of the 3-phase currents, whose expression is given by:

$$I_{\text{max}} = \sqrt{\frac{2}{3}}\sqrt{i_d^2 + i_q^2} \tag{19}$$

When an intensive disturbance occurs, both the d-axis and q-axis voltages are modified to make both the d-axis and q-axis currents converge to zero. By considering:

$$\begin{cases} V_d^{\max} = -p\, y_\Omega\, l_q\, i_q \\ V_q^{\max} = p\, y_\Omega\, (l_d\, i_d + \psi_f) \end{cases} \tag{20}$$

the dq-axis equations of the currents are given by:

$$\begin{cases} l_d\, \dfrac{di_d}{dt} + r_s\, i_d = 0 \\ l_q\, \dfrac{di_q}{dt} + r_s\, i_q = 0 \end{cases} \tag{21}$$

that makes converge them to zero and stops the system.

Figure 10 presents some experimental results obtained for two currents saturation values, $I_q^{sat} = 2\,\text{A}$ and $I_q^{sat} = 1\,\text{A}$. In the two tested cases, the disturbance is identical. The load torque waveform is given by its estimation.

On the left side of the Figure 10, the *passive saturation* of i_q has been fixed to $I_q^{sat} = 2\,\text{A}$. Note that the saturation value for the *active saturation* method has been fixed to $I_q^{sat2} = I_q^{sat} + 20\% \cdot I_q^{sat} = 2.4\,\text{A}$. As regards the *max saturation*, the saturation level is chosen as follows: $I_q^{sat3} = I_q^{sat2} + 30\,\%\, I_q^{sat2} = 3.12\,\text{A}$. According to the figure, when the load torque is applied, only the passive and active methods act. Indeed, there is no point in activating the *max saturation* method because the maximum peak value of the 3-phase currents is not reached (3.12 A).

In order to validate the *max saturation* method, the *passive saturation* value is reduced to $I_q^{sat} = 1\,\text{A}$. Thus, the saturation values for the two other methods are

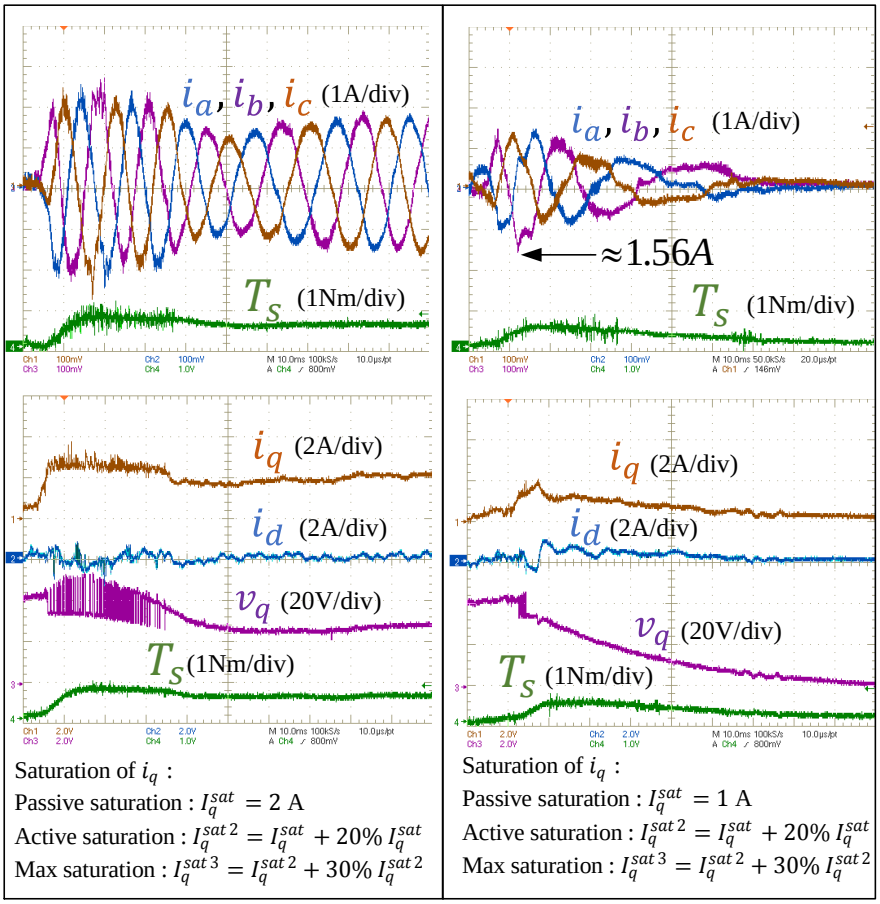

Figure 10. Experimental results presenting two saturation cases with all activated methods (passive, active and max)

given by $I_q^{sat2} = 1.2$ A and $I_q^{sat3} = 1.56$ A. In this case, the results are plotted in the right-side in Figure 10. The excessive saturation value (1 A) simulates a case where the disturbance is intensive. The results show that the *max saturation* method has to be executed in order the q-axis current not to go beyond its saturation value (1.56 A). The system is thus stopped and the regulation is over.

The association of the three presented methods allows protecting the system from disturbances even if one-loop control structure is implemented for the system regulation. Every presented method is important as it acts differently according to given saturation levels.

5. Conclusion

This paper presented a high bandwidth control method based on flatness properties of a system composed of a PMSM fed by a voltage source inverter. This control method offers numerous advantages in terms of transient states. Indeed, all the state or input variables behaviors are analytically known. This control method can be qualified as "large signal" because its implementation is made without any linearization around an operating point of the state model. The second part of that paper focuses on additional protection methods to prevent the system from having an uncontrollable behavior when it faces to disturbances. The proposed protections are based on the variables saturation study, and three additional methods have been implemented: the *passive*, *active* and *max saturation* methods. The first one allows the speed trajectory to be modified so that the considered variables can be passively saturated. The second one acts when the disturbance dynamic is higher than that of the speed regulation. It allows saturating the q-axis current by switching the q-axis voltage between two defined values so that i_q remains in the vicinity of its saturation value. Finally, the third method is a last resort one as its purpose consists in stopping the system when an intensive load torque is applied. Both the simulation and experimental results have validated the proposed control and its different protection methods.

References

Choi J.-W., Lee S.-C. (2009). Antiwindup strategy for pi-type speed controller. *IEEE Transactions on Industrial Electronics*, Vol. 56, No. 6, pp. 2039-2046.

Dannehl J., Fuchs F. (2006). Flatness-based control of an induction machine fed via voltage source inverter - concept, control design and performance analysis. In *Ieee industrial electronics, iecon 2006 - 32nd annual conference on*, p. 5125-5130.

Delaleau E., Stanković A. (2004, June). Flatness-based hierarchical control of the pm synchronous motor. In *American control conference, 2004. proceedings of the 2004*, Vol. 1, p. 65-70 vol.1.

Feng Y., Zheng J., Yu X., Truong N.-V. (2009). Hybrid terminal sliding-mode observer design method for a permanent-magnet synchronous motor control system. *IEEE Transactions on Industrial Electronics*, Vol. 56, No. 9, pp. 3424-3431.

Fliess M., Lévine J., Martin P., Rouchon P. (1995). Flatness and defect of non-linear systems: introductory theory and examples. *International Journal of Control*, Vol. 61, No. 6, pp. 1327-1361. Retrieved from http://www.tandfonline.com/doi/abs/10.1080/00207179508921959

Gensior A., Sira-Ramírez H., Rudolph J., Guldner H. (2009). On some nonlinear current controllers for three-phase boost rectifiers. *IEEE Transactions on Industrial Electronics*, Vol. 56, No. 2, pp. 360-370.

Ghoshal A., John V. (2010, June). Anti-windup schemes for proportional integral and proportional resonant controller. In *National power electronics conference.* Roorkee.

Hagenmeyer V., Delaleau E. (2003). Exact feedforward linearization based on differential flatness. *International Journal of Control*, Vol. 76, No. 6, pp. 537-556. Retrieved from http://www.tandfonline.com/doi/abs/10.1080/0020717031000089570

Houari A., Renaudineau H., Martin J.-P., Pierfederici S., Meibody-Tabar F. (2012). Flatness-based control of three-phase inverter with output lc filter. *IEEE Transactions on Industrial Electronics*, Vol. 59, No. 7, pp. 2890-2897.

Kaiqi Z. (2011). The study of improved pi method for pmsm vector control system based on svpwm. In *Industry applications society annual meeting (ias), 2011 ieee*, p. 1-4.

Lévine J. (2009). *Analysis and control of nonlinear systems: A flatness-based approach*. Springer. Retrieved from http://books.google.fr/books?id=HHRslb_8970C

Malloci I. (2006). *Contrôle anti-windup pour systèmes à commutation*. Unpublished doctoral dissertation, Università degli studi di Cagliari.

Martin P., Murray R., Rouchon P. (2002, January). Flatness based design. *Encyclopedia of Life Support (EOLSS)*, Vol. XIII.

Payman A. (2009). *Contribution à la gestion de l'energie dans les systèmes hybrides multi-sources multi-charges*. Unpublished doctoral dissertation, Institut National Polytechnique de Lorraine.

Payman A., Pierfederici S., Meibody-Tabar F., Davat B. (2011). An adapted control strategy to minimize dc-bus capacitors of a parallel fuel cell/ultracapacitor hybrid system. *Power Electronics, IEEE Transactions on*, Vol. 26, No. 12, pp. 3843-3852.

Richter S., De Doncker R. (2011). Digital proportional-resonant (pr) control with anti-windup applied to a voltage-source inverter. In *Power electronics and applications (epe 2011), proceedings of the 2011-14th european conference on*, p. 1-10.

Shin H.-B., Park J.-G. (2012). Anti-windup pid controller with integral state predictor for variable-speed motor drives. *IEEE Transactions on Industrial Electronics*, Vol. 59, No. 3, pp. 1509-1516.

Su Y., Zheng C., Duan B. Y. (2005). Automatic disturbances rejection controller for precise motion control of permanent-magnet synchronous motors. *IEEE Transactions on Industrial Electronics*, Vol. 52, No. 3, pp. 814-823.

Zhang X., Sun L., Zhao K., Sun L. (2013). Nonlinear speed control for pmsm system using sliding-mode control and disturbance compensation techniques. *IEEE Transactions on Power Electronics*, Vol. 28, No. 3, pp. 1358-1365.